SAND2005-7892C

Microstructural Evolution in Electronic 63Sn-37Pb/Cu Solder Joints

P.T. Vianco, J.A. Rejent, and A.C. Kilgo
Sandia National Laboratories, Albuquerque, NM USA
ptvianc@sandia.gov; 505-844-3429
jarejen@sandia.gov; 505-844-6341
ackilgo@sandia.gov; 505-844-7634

Abstract

The 63Sn-37Pb (wt.%, designated Sn-Pb) solder interconnections made to copper (Cu) pads were examined on two printed wiring assemblies (PWAs) that had been in the field for 17 years and subsequently exposed to an accelerated aging test environment. A qualitative assessment of the solder joints indicated that there was excellent solderability of the pins and Cu pads. Void formation was minimal or did not occur at all. Manufacturing defects were limited to minor Cu pad lifting with cracks in the underlying epoxy resin and local areas of Cu barrel separation from the laminate hole wall. Both defects would not have influenced the effects of the accelerated aging environment. A quantitative analysis examined the intermetallic compound (IMC) layer thickness of selected components on the PWAs. The IMC thickness data indicated that the PWAs were exposed to considerably lower, cumulative temperatures inside the product assembly than were present outside as a result of the accelerated aging environment. The quantitative analysis also evaluated the Pb-rich phase particle size in both fillets and the hole region of the PWA solder joints. The Pb-rich phase size confirmed that the temperature environment at the PWA level was significantly less severe than that of the accelerated aging environment. The Pb-rich phase size data indicated that the solder joints were exposed to a limited degree of thermal mechanical fatigue (TMF) that likely originated from the nominal temperature fluctuations coupled with the thermal expansion of the encapsulant as well as large expansion of the circuit board laminate in the z-axis (through-thickness) direction. This study demonstrated the methodology by which, IMC thickness and Pb-rich phase size were used to assess the temperature/time conditions experienced at the Sn-Pb/Cu interconnection level versus the external environment.

Introduction

The microstructure of the 63Sn-37Pb solder (wt.%, abbreviated Sn-Pb) is dependent upon two factors: (1) the initial processing conditions that generated the material from the molten state, specifically, the *cooling rate*, and (2) the thermal-mechanical environment to which the material was exposed during its life cycle after solidification. Shown in Fig. 1 is the microstructure of the Sn-Pb solder. It is comprised of Pb-rich phase particles in a Sn-rich matrix. Per the binary phase diagram, there is no significant solubility for Pb in the Sn-rich phase and approximately 3 wt.% solubility of Sn in the Pb-rich phase at 25°C.

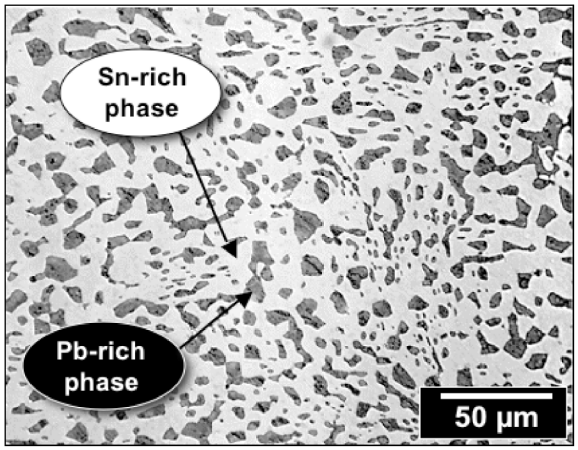

Figure 1. Optical micrograph showing the microstructure of the Sn-Pb eutectic alloy.

Regarding point (1), previous studies have described the sensitivity of the starting microstructure to the cooling rate as well as the impact of initial microstructure and thusly, cooling rate, on the solder mechanical properties [1 - 6]. The microstructural metric was the size of the Pb-rich phase particles. The faster was the cooling rate, the finer were the Pb-rich phase particles and visa-versa.

With respect to point (2), the Pb-rich phase particles change morphology – primarily size than shape – under the thermal mechanical environment(s) of the solder joint. There are two contributing factors. First, there is the effect of temperature. Generally, the Pb-rich phase coarsens when exposed to elevated temperatures. Even room temperature (25°C) is considered a relatively high temperature for Sn-Pb solder. Based upon the homologous temperature, T_h, which is the ratio, T_e/T_s, where T_e is the environmental temperature (K) and T_s is the solidus temperature (K), room temperature represents $T_h = 0.65$. This value is equivalent to exposing a Ni-based superalloy to the combustor section of an operating jet engine. At 25°C, the extent of coarsening is more limited than at elevated temperatures [2]. Nevertheless, measurable changes have been observed in the hardness of Sn-Pb based solders after room temperature aging, implying that

microstructural changes in addition to Pb-rich phase coarsening may occur in the Sn-Pb alloy [6].

The second contributing factor towards Pb-rich phase size is deformation. So-called strain-enhanced coarsening is the signature effect of thermal mechanical fatigue (TMF) of Sn-Pb solder interconnections used on electronics assemblies [7]. This phenomenon is illustrated in Fig. 2. The sequence of pictures began with the as-fabricated condition in Fig. 2(a). Coarsening was evident in Fig. 2(b). The Pb-rich phase coarsening eventually led to crack development as shown in Fig. 2(c).

Because TMF is, by its nature, an elevated temperature phenomenon, there are actually two contributions to the Pb-rich phase coarsening: temperature and deformation. In order to simplify the computational modeling of TMF in Sn-Pb solder joints, it has been assumed that these two effects can be addressed independently, and that their respective effects on Pb-rich phase coarsening are additive [8].

In the absence of deformation, the extent of Pb-rich phase coarsening will depend strictly upon the temperature and time history. The total coarsening that results from multiple temperature conditions could be determined by the addition of particle growth in each of the individual stages. Thus, the Pb-rich phase particle coarsening parameter provides a quantitative metric of the cumulative temperature history to which the solder (joint) was exposed. As a thermally activated process, the Arrhenius expression can predict particle coarsening as a function of temperature and time.

An Arrhenius equation was developed, which predicts the extent of Pb-rich phase coarsening as a function of temperature and time [9]. The expression that is applicable to the temperature range of 25°C – 100°C, is shown as equation (1) below. The parameter, y, is Pb-rich phase particle area (mm^2):

$$y\ (mm^2) = 3.2 \times 10^{-6} + 0.00147\ t^{0.32} \exp[-31000/RT] \qquad (1)$$

where 3.2×10^{-6} mm^2 is the initial Pb-rich phase size; 0.00147 is a constant; 0.32 is the time exponent (constant); 31000 J/mol is the apparent activation energy; R is the universal gas constant, 8.314 J/mol-K; and T is temperature (K). Confirmation of the kinetics parameters in equation (1) was provided in the more detailed study cited in reference 2, using the reasonable assumption of a cooling rate of 10 – 100 °C/min for the solder joints. The initial Pb-rich phase size was determined from the earlier analysis of hand-soldered, through-hole solder joints [9].

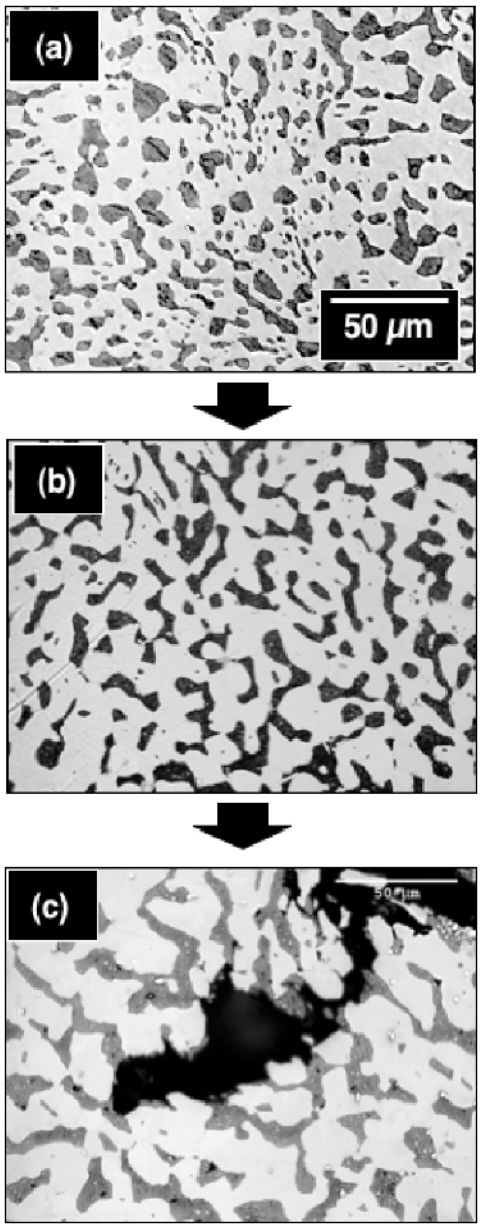

Figure 2. Optical micrographs illustrating strain-enhanced, Pb-rich phase coarsening in Sn-Pb that has undergone TMF: (a) as-fabricated condition; (b) Pb-rich phase coarsening; and (c) crack development within the coarsened regions.

A drawback to the use of the Pb-rich phase size as a metric for the cumulative temperature history of the solder joint remains the contribution of strain-enhanced coarsening due to deformation – the specific case being TMF. Therefore, a second metric was established, which was not sensitive to deformation. That metric was the thickness of the intermetallic compound (IMC) layer that forms between Sn-Pb solder and the Cu base material. An optical micrograph showing the layer in the as-soldered condition is shown in Fig. 3. The specific stoichiometry of the IMC layer was Cu_6Sn_5.

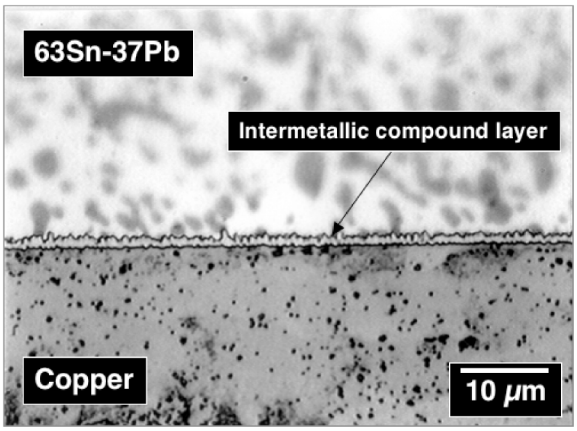

Figure 3. Optical micrograph showing the as-soldered IMC layer that formed between Sn-Pb solder and Cu.

It was determined in a previous investigation that IMC growth in the Sn-Pb/Cu system was not sensitive to an applied stress and any associated deformation [10]. The IMC growth can be predicted from the kinetics expression shown in equation (2) below:

$$x\ (\mu m) = 0.71 + 0.0032\ t^{0.58} \exp[-52200/RT] \qquad (2)$$

where x (μm) is the layer thickness at time, t (s); 0.71 is the initial thickness (μm); R is the universal gas constant, 8.314 J/mol-K; and T is the temperature (K). The two kinetics parameters are the time exponent, 0.58±0.07 and the apparent activation energy (ΔH), 52200±8500 J/mol. The initial IMC layer thickness, 0.71 μm, is not particularly sensitive to the overall soldering process (time above liquidus, cooling rate, etc.) [9].

The present study was undertaken to assess the extent of aging that occurred in the solder joints of printed wiring assemblies (PWA) in a product assembly. Specifically, the objective was to determine the degree to which, the PWAs contained in the product housing had experienced the (external) time-temperature conditions of the accelerated aging profile. Lead-rich phase coarsening and thickness of the Cu_6Sn_5 IMC layer were the quantitative metrics used to determine the actual time-temperature conditions experienced by the PWA solder joints.

Experimental Procedures

Printed Wiring Assemblies

The PWAs that were used in the present study were from the product assembly designated S/N1244. Shown in Fig. 4 are stereo photographs showing (a) the top (component) side and (b) the bottom side of the PWA designated A201. The PWA was encapsulated in a polyurethane hard "potting" foam. Mechanical techniques were used to remove the foam from both sides of the PWA. Both solder joints were evaluated on each of the six components indicated in Fig. 4(b). The "R" designation was for wire-wound resistors and "CR" indicated diodes. The corresponding lines showed the location of the metallographic cross section through the corresponding interconnections.

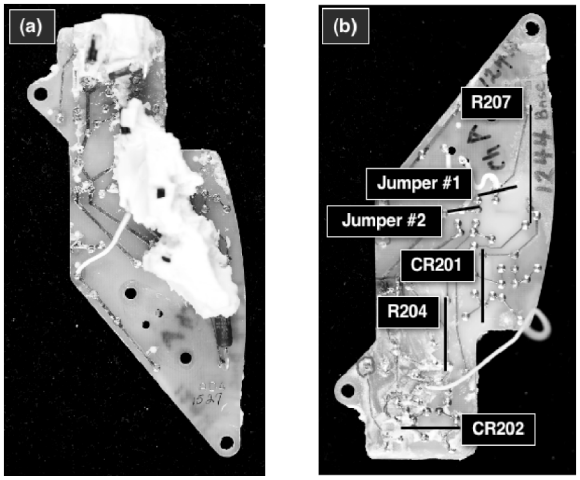

Figure 4. Stereo photographs showing (a) the top (component) side and (b) the bottom side of the A201 PWA test vehicle. The encapsulant material had been partially removed for component identification, which was provided in (b).

A second PWA from S/N1244, designated B201, was also evaluated in this study; its appearance was very similar to that of the A201 unit in Fig. 4. The same components were evaluated, as well.

The same two PWAs, A201 and B201, were also examined, which were extracted from the product assembly designated S/N1192. The analysis of these PWAs provided the baseline data because they were not exposed to the accelerated aging conditions.

PWA History

The PWAs were installed into the two product units, S/N1192 and S/N1244, which were then placed into the field for 17 years. The units were retrieved from the field. The assembly S/N1192 was immediately disassembled to extract the PWAs for analysis. The second product assembly, S/N1244, was placed, in its entirety, into the accelerated aging test chamber. That is, the PWAs were *not* removed from the unit prior to exposure to the conditions described below.

The total accelerated aging environment was comprised of two temperature/time profile segments that were administered in series. Those profiles are listed below:

Temperature/Time Profile #1:

1. 30°C (86°F) …….. 20 hours
2. 71°C (160°F) …… 500 hours
3. *Eleven (11) cycles:*
   a. 71°C (160°F) to –54°C (-65°F) …… 12 hours
   b. –54°C (-65°F) …….. 24 hours
   c. -54°C (-65°F) to 71°C (160°F) ……. 12 hours
   d. 71°C (160°F) …… 24 hours

Temperature/Time Profile #2:

1. 25°C (77°F) to –54°C (-65°F) …….. 12 hours
2. -54°C (-65°F) ……24 hours
3. –54°C (-65°F) to 30°C (86°F) …….. 12 hours
4. 30°C (86°F) …….. 34 hours
5. *Fifteen (15) cycles*:
   a. 30°C (86°F) to 60°C 140°F) ……..... 17 hours
   b. 60°C (140°F) to 31°C (86°F) …… 17 hours

6. 31°C (86°F) ……...100 hours

This combined environment accelerated the effects of both static (isothermal) and fluctuating temperature conditions that were predicted to occur over the service life of the product assembly. Between the two temperature/time profiles, the unit was removed from the chamber for functional testing. Those tests were performed at 25°C (77°F), -54°C (-65°F), and 71°C (160°F). The time during which the unit was held at these temperatures was deemed negligible with respect to the aging cycles.

Upon the completion of the accelerated aging treatment, the S/N1244 unit was removed from the chamber and disassembled to the level of the PWAs shown in Fig. 4. Metallographic cross sections were performed on the designated solder joints. Initially, the cross sections were evaluated, qualitatively, in order to identify the materials comprising the leads, coatings, and circuit board structures as well as to assess the overall integrity of the interconnections. There were two objectives, here. First, the assessment searched for signs of degradation that may have been caused by the temperature/time profiles. Such degradation included excessive deformation or cracks in the solder. Secondly, this exercise also examined the solder joints for manufacturing defects. Those defects, which included excessive void formation, damage to the laminate, and/or delamination at any one of a number of interfaces, could have potentially affected the response of the interconnection to the accelerated aging conditions.

Intermetallic Compound (IMC) Layer Thickness and Pb-Rich Phase Particle Size Analyses

The schematic diagram in Fig. 5 shows the location of the IMC layer thickness and the Pb-rich phase size measurements. Note the designation of the top (component) side and the bottom side. The IMC layer thickness was determined from 1000x magnification optical micrographs of the solder/Cu pad interface. Micrographs were taken at two locations, one at the top side fillet and the other at the bottom side fillet of both leads per component. Thirteen measurements were made per each photograph. Those data were combined from the two locations of both solder joints to provide a single value that was representative of a particular device. (Prior analyses indicated very little difference in IMC layer thickness between the top and bottom surfaces.)

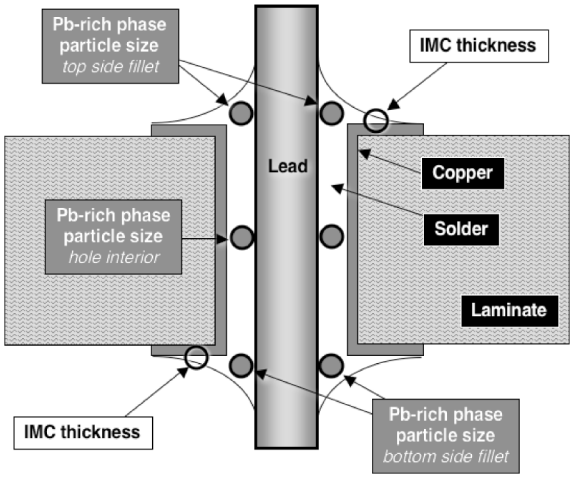

Figure 5. Schematic diagram showing the location of the IMC thickness and Pb-rich phase particle size measurements.

The Pb-rich phase particle size measurements were made on the solder joints of both leads per each component. Optical micrographs were taken at six sites, using a 500x magnification. Two micrographs were taken at each of the following three locations (Fig. 5): (1) top (component) side fillet; (2) hole interior; and (3) bottom side fillet. Quantitative image analysis determined the particle size distributions based upon particle area (mm^2). The specific statistical parameters of interest were: mean area; standard deviation; total number of particles evaluated; maximum area; and area percent that was Pb-rich phase in the microstructure. It is important to realize that the standard deviation reflects the *spread in the size of the Pb-rich phase particles*. It does not represent the error term on the mean of the particle size measurement. That parameter was the 95% confidence interval. In fact, the 95% confidence interval, as an error term, was very small, owing to the large number of particles used in the analyses, which was between 800 and 4000 particles.

The analysis of the Pb-rich phase data was performed with the following methodology: First, the Pb-rich phase size measurements were combined from the two pictures, per each of the three locations on a joint. Then, the Pb-rich phase size measurements, which corresponded to each of the three joint locations, were combined together from the two leads. The result was three sets of Pb-rich phase particle size statistics, one for each of the three locations, representing the particular component.

The quantity of Pb-rich phase that was present in the microstructure was also evaluated from the micrographs. This exercise was required because the coarsening kinetics analysis were specific to the 63Sn-37Pb and 60Sn-40Pb compositions, only. The assumption was made that, given a random distribution of particles and an absence of any one preferred orientation, the volume percent of Pb equaled the measured area percent value. Therefore, the conversion of the 63Sn-37Pb between weight percent and area or volume percent was:

63Sn-37Pb (wt.%) ⇐⇒ 72.6Sn-27.4Pb (area%) (3)

The nominal Pb weight percent values were corrected for the solid solution of Sn in the particles; therefore, a value of 3 wt.% was subtracted from that nominal percent.

Results and Discussion

Qualitative Observations of the Solder Joints

The discussion will concentrate upon the PWAs from S/N1244, which were exposed to the accelerated aging environment. Where applicable, comparisons will be made to the PWAs from the baseline S/N1192 assembly. In general, the PWAs exhibited excellent workmanship, having a minimum occurrence of voids and adequate solderability of the component leads and circuit board Cu features. There was an absence of damage to the component leads or to the laminate. There was Cu pad lifting observed under the solder fillet, which was also accompanied by a limited amount of laminate (resin) cracking under the pad. This phenomenon was illustrated by the optical micrographs in Fig. 6, which were from one of the two solder joints belonging to the R204 resistor on the A201 PWA. A low magnification micrograph of the joint was provided in Fig. 6(a). The high magnification micrographs provided in Figs. 6(b) and 6(c) illustrated the degree of cracking in the laminate resin under the Cu bond pads. The limited severity of this damage would not jeopardize the long-term reliability of the interconnections and, certainly, did not affect the quantitative metrics of IMC layer thickness or Pb-rich phase coarsening in the solder joints.

Lifting of the Cu pad and laminate cracking were also observed to a similar extent in the solder joints of the same PWAs from the S/N1192 baseline unit. Lifting of Cu pad is typically considered a manufacturing defect. It is often the result of heat damage to the laminate during the soldering process, in particular, when joints are assembled by hand soldering with an electric iron, which was the process for these PWAs. A contributing factor could have also been the high z-axis (through-thickness) thermal expansion of the laminate relative to that of other materials comprising the joint, that is, the Sn-Pb solder, the Cu or Fe-alloy lead, and the Cu conductor.

A second phenomenon that was observed in the cross sections was separation of the Cu barrel layer from the laminate hole wall. The optical micrographs that were provided in Fig. 7 exemplified the degrees to which this separation took place. In this particular solder joint, the Cu barrel separation was observed similarly on the other side of the joint.

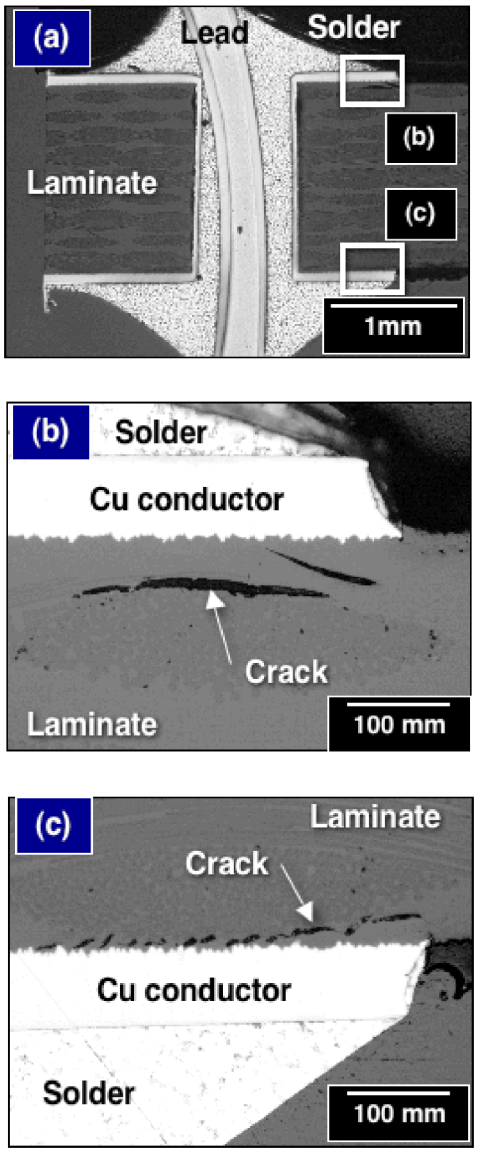

Figure 6. (a) Low magnification, optical micrograph showing the section of one of two R204 solder joints from the A201 PWA. (b, c) High magnification, optical micrographs showing cracking of the laminate resin and lifting of the Cu pad.

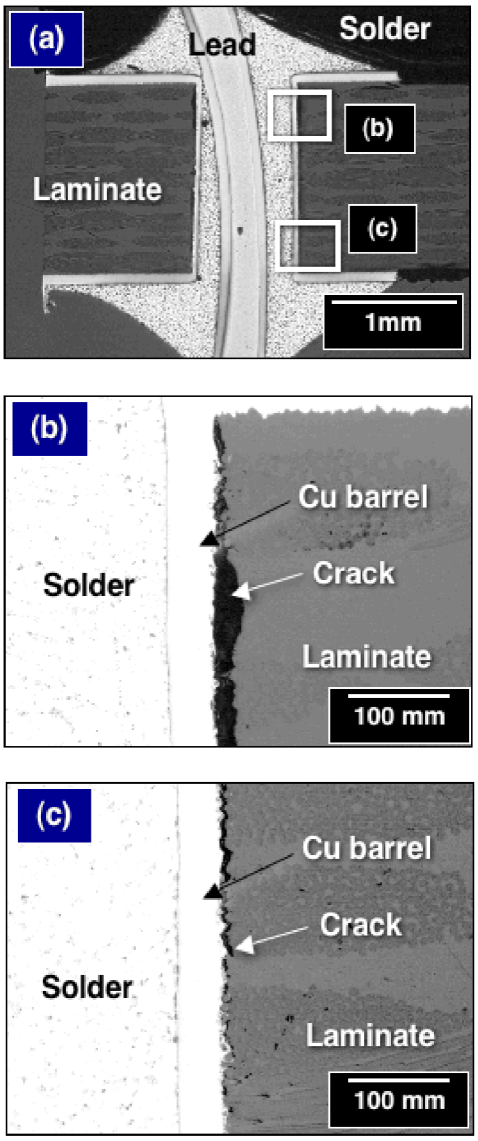

Figure 7. (a) Low magnification, optical micrograph showing the section of one of two R204 solder joints from the A201 PWA. (b, c) High magnification, optical micrographs showing the extents of separation of the Cu barrel layer from the hole wall.

The separation was greatest on the component side (Fig. 7 (b)), but then diminished with distance towards the bottom side (Fig. 7 (c)). The separation was most frequently observed at those locations where the Cu layer was joined to the epoxy resin of the laminate. The separation of the Cu layer from the laminate did not cause fracture of the former, nor fracture at the junction between the Cu barrel layer and the Cu pad on either surface.

Separation of the Cu barrel layer from the laminate hole wall was not observed in the solder joints of the PWAs from the baseline unit, S/N1192. However, this phenomenon was not likely to have been caused by the accelerated aging environment. Interfacial delamination in circuit board structures is typically a manufacturing defect. The causes are many, including smearing of the laminate components during the drilling process that degrades adhesion of the Cu to the hole wall. The most predominant cause of Cu/laminate delamination is the vaporization of residual moisture, which was trapped between the Cu layer and the laminate, during the soldering process. Irrespective of the root-cause, the limited prevalence and severity of the separation would not have affected the long-term mechanical or electrical performance of the solder joints, especially since there were no internal conductive layers in the laminate. Also, Cu barrel separation was not sufficiently extensive so that it would have changed the effects of the accelerated aging conditions on the IMC layer thickness or Pb-rich phase coarsening metrics.

Quantitative Analyses

The IMC thickness data were compiled in Table 1 for both the A201 and B201 PWAs from the unit S/N1244 after accelerated aging. Only the Cu_6Sn_5 composition was observed along the Sn-Pb/Cu interfaces. The IMC layers were not particularly thick and would have certainly not resulted in a loss of interconnection reliability or the capacity for the interconnection to be reworked and/or repaired.

Table 1. IMC Layer Thickness for Solder Joints from the S/N1244 Unit After Accelerated Aging.

PWA	Component	Cu_6Sn_5 IMC Thickness (μm)
A201	CR201	0.86±0.34
A201	CR202	0.85±0.24
A201	R204	0.98±0.31
A201	R207	1.10±0.32
B201	CR201	0.87±0.26
B201	CR202	0.95±0.34
B201	R204	0.89±0.34
B201	R207	0.98±0.34

A comparison was made between the IMC layer thicknesses from the aged solder joints (Table 1) and similar data from the PWAs of the baseline S/N1192 product assembly. The two data sets were plotted in Fig. 8. (The designation, AAU, refers to accelerated aging unit, that is, the S/N1244 unit used in the present study.) The error bars represented one standard deviation. The mean IMC thicknesses were higher for the S/N1244 unit as expected, since the PWAs were exposed to the higher temperatures of the accelerated aging conditions. However, the differences between the two units were not considered to be large; in fact, they were not statistically significant based upon the standard deviation values[1]. It was not expected that trends of IMC versus component type would have been observed in the two data sets because the relatively small IMC thicknesses in both cases obscured such trends.

[1] Hypothesis testing (F-test and Student's t-test) was not performed on the IMC data to establish a confidence interval. However, such procedures have been established and used successfully in these analyses [9].

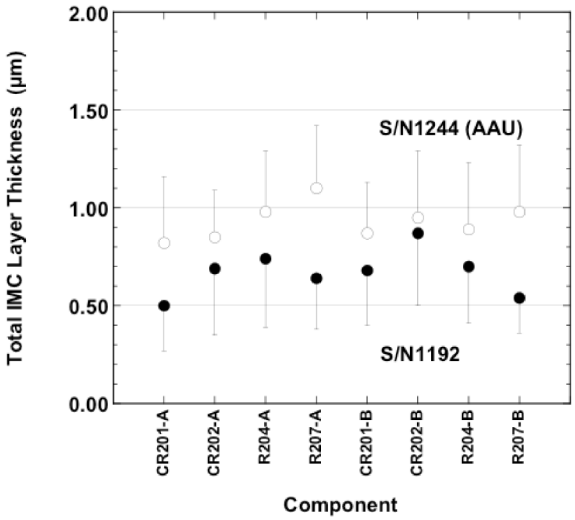

Figure 8. Plot of IMC thickness as a function of component type for the PWAs A201 and B201 from the S/N1192 (baseline) and S/N1244 (accelerated aging unit, or AAU) product assemblies.

The Pb-rich phase size data were obtained from the solder joints on the A201 and B201 PWAs of the S/N1244 aged unit. The data from components on the A201 PWA were listed in Table 2; similar results were obtained from the B201 solder joints. The mean values were accompanied by error terms based upon the 95% confidence intervals. Also the tables included the total number of particles used in each analysis as well as the weight percent of Pb-rich phase represented by those particles. The latter parameter was corrected for the assumed 3 wt.% of Sn contained in the Pb-rich phase. It was observed that the weight percent Pb values indicated that the 60Sn-40Pb solder was used to make the interconnections. The rate kinetics expression for coarsening, equation (2), was suitable for this alloy as well as for the 63Sn-37Pb eutectic composition as was noted earlier.

The Pb-rich phase size data shown in Table 2, as well as that pertaining to the B201 PWA, were compared to the non-aged PWAs (S/N1192) in Figs. 9 – 11. Shown in Fig. 9 is the plot of Pb-rich phase particle size as a function of component for the fillet top (component side) location.

Table 2. Pb-Rich Phase Particle Data for Solder Joints from the A201 PWA of the S/N1244 Unit After Accelerated Aging.

PWA	Component	Location	Mean Pb-rich Particle Area ± 95% CI ($x10^{-6}$ mm^2)	Number of Particles	Weight Percent of Pb *(corrected)* (%)
A201	CR201	Fillet, Top	13.8±1.1	2588	40
		Hole	14.7±2.0	1039	39
		Fillet, Bottom	13.1±1.2	2910	41
A201	CR202	Fillet, Top	11.1±0.9	3243	41
		Hole	16.9±2.2	1003	40
		Fillet, Bottom	10.1±0.8	3546	41
A201	R204	Fillet, Top	10.2±1.0	3137	37
		Hole	17.6±1.9	1063	36
		Fillet, Bottom	12.0±1.1	2731	37
A201	R207	Fillet, Top	12.1±1.4	2868	39
		Hole	19.4±3.0	867	40
		Fillet, Bottom	12.7±1.2	2895	40

The first observation was the large degree to which, the phase size varied between the A201 and B201 PWAs on either S/N unit. This variation was not unexpected for fillets on the component side because the soldering process takes place on the opposite (bottom) side. The molten solder had to flow through the hole, reaching the top side where solidification took place in a less controlled manner, owing to the remoteness of the heat source and the varying heat sink effect of component leads and the laminate.

A second observation was that the accelerated aging condition caused little change to the Pb-rich phase size of the A201 PWA solder joints when compared to the corresponding joint of the baseline PWA (S/N1192). On the other hand, there was a dramatic increase in the Pb-rich phase size of the B201 PWA solder joints. The IMC data did not indicate that the A201 and B201 PWAs were exposed to drastically different cumulative temperature environments (Fig. 8). Therefore, it was concluded that there was a greater contribution of strain-enhanced coarsening in the B201 solder joints. The source of the added coarsening was likely the additional stresses generated by the encapsulant material. Local differences in encapsulant geometry as well as intrinsic materials properties caused by varying foam densities (i.e., thermal expansion coefficient or elastic modulus) resulted in different localized stresses amongst the PWA interconnections. Moreover, encapsulant effects would be expected to be more significant on the top side fillet because the encapsulant can interact with the entire component body, resulting in a bending action on

the lead that generated the additional coarsening in the solder fillet.

A third observation was that the 95% confidence intervals (i.e., the error terms) scaled with the mean Pb-rich phase particle size. This effect was a possible consequence of the log-normal distribution that characterizes the Pb-rich phase particle distribution. A higher mean can be accompanied by a wider spread in the particle size distribution, thereby causing an increase in the confidence interval. This trend was observed for the Pb-rich phase particle sizes measured in the hole and bottom side fillet locations, as well.

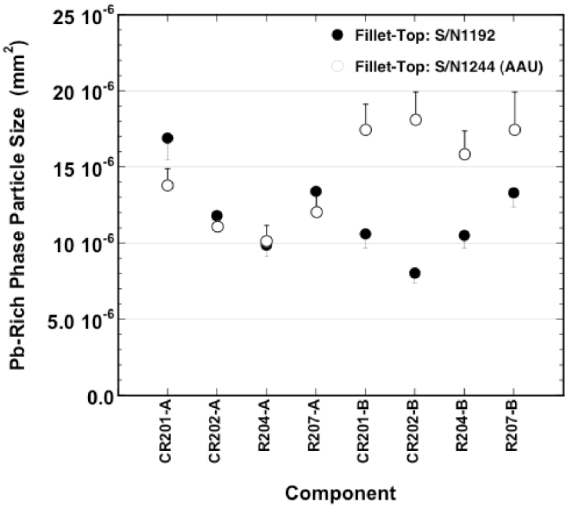

Figure 9. Graph of Pb-rich phase particle size as a function of component on the A201 (-A) and B201 (-B) PWAs from product assemblies S/N1192 (baseline) and S/N1244 (AAU) for the top (component) side fillet.

Next, the Pb-rich phase particle size values were examined for the hole region; those data are presented in Fig. 10. In prior investigations, it was observed that the Pb-rich phase size data tended to be more scattered in the hole area. First of all, there is a limited quantity of solder to analyze for the particle size distribution. Secondly, the solidification process will be variable due to variations in the configuration of the lead vis-à-vis the laminate wall. The present data showed a similar behavior. The accelerated aging environment caused larger Pb-rich phase particle sizes (S/N1244) when compared to the as-received case (S/N1192), except for the first two components on the A201 PWA. In those two cases, the lack of difference between aged (S/N1244) and unaged (S/N1192) cases was caused by the S/N1192 particle sizes being uncharacteristically larger than other joints on either the same PWA or the sister PWA, B201.

Also, the potential for strain-enhanced coarsening is high within the solder joint hole. There, the differences in thermal expansion mismatch are particularly large between the component lead and the circuit board laminate because of the latter's very high z-axis (through-hole) thermal expansion coefficient. It was likely that this thermal expansion mismatch caused a greater degree of Pb-rich phase size coarsening than occurred at the other two fillet locations.

The Pb-rich phase particle sizes, which were measured at the bottom side fillets, were shown in Fig. 11. The S/N1244 data showed generally reduced magnitudes versus the other two locations, as well as less variability amongst the solder joints within each of the A201 and B201 PWAs, or between the two PWAs. Similar trends were observed for solder joints on the PWAs of the baseline S/N1192 unit. The reduced variability was associated with the heat source having been located there during the soldering process. Upon removal of the heat source, the rapid cooling rate experienced by the solder caused less variability in the as-solidified microstructures generated in the solder joints between the various components.

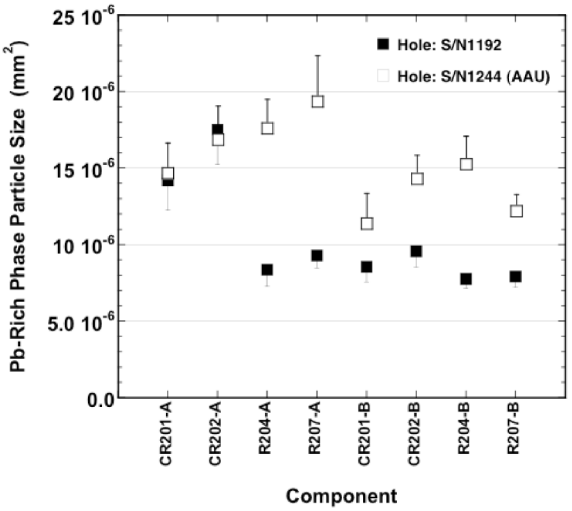

Figure 10. Graph of Pb-rich phase particle size as a function of component on the A201 (-A) and B201 (-B) PWAs from product assemblies S/N1192 (baseline) and S/N1244 (AAU) for the solder joint hole region.

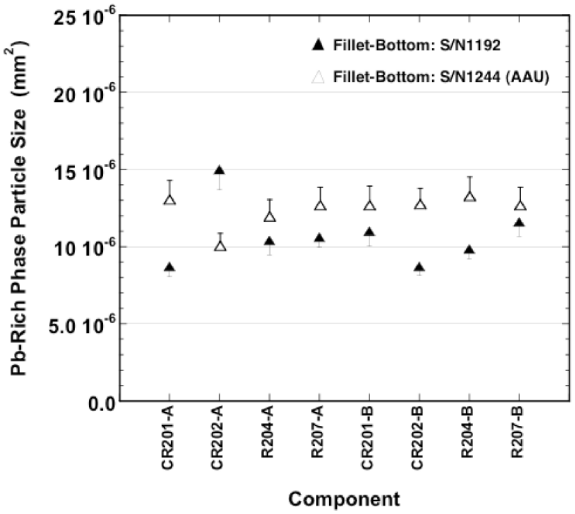

Figure 11. Graph of Pb-rich phase particle size as a function of component on the A201 (-A) and B201 (-B) PWAs from product assemblies S/N1192 (baseline) and S/N1244 (AAU) for the solder joint bottom side fillet region.

Also, a smaller Pb-rich phase particle size in bottom side fillets was caused by a reduced degree of strain enhanced coarsening. The effect of the encapsulant occurred to a lesser degree in the bottom side of the solder joints. Therefore, it was expected that coarsening of the Pb-rich phase particles in the bottom fillets of the aged solder joints (S/N1244) would be less affected by strain-enhanced coarsening. Thus, the particle sizes would more closely reflect the cumulative temperature-time history of the solder joint. To this effect, it was observed in Fig. 11 that, with the exception of CR202 component on the A201 PWA, the S/N1244 AAU exhibited only slightly larger particle sizes than were those of comparable joints of the PWAs from the baseline S/N1192 unit.

An analysis was performed, which compared the IMC layer thickness and Pb-rich phase particle size data obtained from the solder joints of the aged S/N 1244 PWAs against the corresponding metrics that were predicted by the kinetics equations (1) and (2), respectively, per the accelerated aging time-temperature history described in the experimental procedures section. Specifically, the IMC layer thickness and Pb-rich phase size values were predicted from those two equations by dividing the two accelerated aging profiles into 6C° to 10C° temperature increments. The median temperature within each such increment was used to compute the extent of IMC layer growth or Pb-rich phase particle coarsening using equations (1) and (2), respectively. Cumulative IMC layer thicknesses or Pb-rich phase sizes were tallied at each step. Final values were determined at the end of the accelerated aging sequence. Recall that the predicted Pb-rich phase size took into account only the effect of temperature; there is no accounting for the TMF contribution to Pb-rich phase coarsening.

Shown in Fig. 12 is a graph of the cumulative IMC layer thickness (left ordinate) and Pb-rich phase size values (right ordinate) that were predicted through the sequence of steps compiled for the accelerated aging environment. The arrows point to the respective ordinates. The term, "predicted", indicates that these results were calculated by equations (1) and (2) above. The respective experimental data of IMC layer thickness and Pb-rich phase particle size (for the three solder joint locations) were combined from all components on the aged A201 and B201 PWAs from the S/N1244 unit. The resulting values were represented by the cross hatched box next to the relevant y-axis. The top and bottom edges of the boxes were the maximum and minimum limits, respectively, of each data set.

It was apparent in Fig. 12 that the experimentally measured IMC growth and Pb-rich phase size values from the S/N1244 solder joints were considerably less than those predicted from equations (1) and (2), respectively, according to the accelerated aging conditions. It was concluded that the accelerated aging environment did not reach the PWAs when they were contained in the product assembly. It was surmised that the housing and encapsulant formed an insulating barrier between the PWAs and the accelerated aging temperatures.

This case study demonstrated that the Pb-rich phase particle size of Sn-Pb solder, as well as the thickness of the Cu_6Sn_5

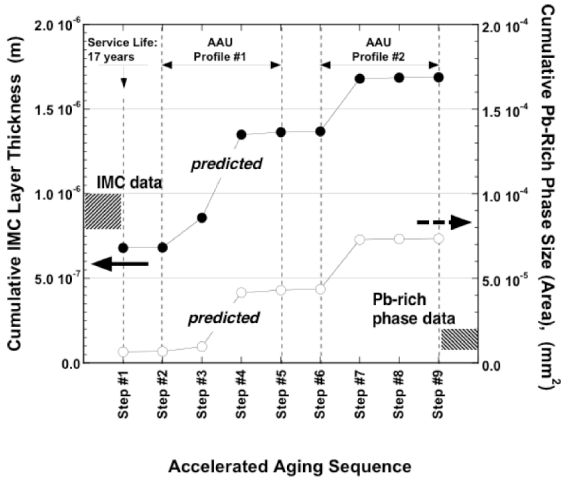

Figure 12. Graph of the cumulative IMC layer thickness (left ordinate) and Pb-rich phase size values that were predicted from the sequence of steps comprising the accelerated aging environment. The arrows point to the respective ordinates. The respective experimental data of IMC layer thickness and Pb-rich phase particle size appear as the cross-hatched boxes

IMC layer at the Sn-Pb/Cu interface, are suitable quantitative metrics for determining the cumulative temperature environments experienced by Sn-Pb solder in an interconnection. In addition, by separating out the effects of temperature alone (IMC layer thickness) and the combination of temperature and strain (Pb-rich phase size), it was possible to ascertain the potential role of TMF on the long-term reliability of these solder joints.

Conclusions

1. The 63Sn-37Pb solder (wt.%, designated Sn-Pb) interconnections made to copper (Cu) pads were examined on two printed wiring assemblies (PWAs) that had been in the field for 17 years and subsequently exposed to an accelerated aging test environment. A qualitative evaluation was made of the solder joints to detect damage resulting from the field service and accelerated aging environment. Quantitative analyses were performed, which measured the Cu_6Sn_5 intermetallic compound (IMC) layer thickness at the Sn-Pb/Cu interface and Pb-rich phase particle size within the solder joint, as a means to determine the cumulative temperature experienced at the interconnection level.
2. The qualitative evaluation indicated that there was excellent solderability of the pins and Cu pads. Void formation was minimal or did not occur at all. Manufacturing defects were limited to minor degrees of Cu pad lifting with cracks in the underlying epoxy resin and local areas of Cu barrel separation from the laminate hole wall. Both defects were not sufficiently severe so as to have skewed the effects of the accelerated aging environment or to jeopardize the long-term reliability of the interconnections.
3. The measured IMC thicknesses, which in-and-of-themselves would not degrade the reliability of the

interconnections nor impact subsequent rework/repair activities, did indicated that the PWAs were exposed to considerably lower, cumulative temperatures than were provided by the accelerated aging environment. The insulating effects of the encapsulant and other product structure reduced the temperature excursions experienced at the PWA solder joint level.

4. The quantitative analysis also evaluated the Pb-rich phase particle size in both fillets and the hole region of the PWA solder joints. The Pb-rich phase size also indicated that the temperature environment at the PWA level was significantly less severe than that of the accelerated aging environment. The Pb-rich phase size data also showed that the solder joints were exposed to a limited degree of thermal mechanical fatigue (TMF) that was likely originated by the presence of the encapsulant as well as from the high z-axis expansion property of the circuit board laminate.

Acknowledgments

The authors wish to thank Mike Kelly for providing the aged PWAs and Don Susan for this thorough review of the manuscript. [1]Sandia is a multiprogram laboratory operated by Sandia Corporation, a Lockheed Martin Company, for the US Dept. of Energy's National Nuclear Security Administration under Contract DE-AC04-94AL85000

References

[1] Nylen, M., and Norgren, S. "Temperature Variations in Soldering and Their Influence on Microstructure and Strength of Solder Joints. *Soldering and Surface Mount Technology*, No. 5 (June), (1990,) pp. 15.

[2] Vianco, P., Rejent, J., Zender, G., and Kilgo, A., "Kinetics of Pb-Rich Phase Particle Coarsening in Sn-Pb Solder Under Isothermal Annealing – Cooling Rate Dependence," *Journal of Materials Research* Vol. 20 (2005), pp. 1463 – 1573.

[3] Guo, Z. and Conrad, H., "Effect of Microstructure Size on Deformation Kinetics and Thermo-Mechanical Fatigue of 63Sn-37Pb Solder Joints", *Journal of. Electronic Packaging* Vol. 118, (1996), p. 49.

[4] Mei, Z., Morris, J., Shine, M., and Summers, T., "Effects of Cooling Rate on Mechanical Properties of Near-Eutectic Tin-Lead Solder Joint," *Journal of Electronic Materials*, Vol. 20, (1991), p. 599.

[5] Rack, H. and Maurin, J., "Mechanical Properties of Cast Tin-Lead Solder", *Journal of Testing and Evaluation*, Vol. 2 (1974), p. 351.

[6] Lampe, B., "Room Temperature Aging Properties of Some Solder Alloys", *Welding Journal, Research Supplement* Vol. 55 (1976), p. 330-s.

[7] Frear, D., "Thermomechanical Fatigue in Solder Materials," Solder Mechanics: A State of the Art Assessment, eds. D. Frear, et al., TMS (Warrendale, PA, 1991), pp. 191.

[8] Vianco, P., Burchett, S., Neilsen, M., Rejent, J., and Frear, D., "Coarsening of the Sn-Pb Solder Microstructure in Constitutive Model-Based Predictions of Solder Joint Thermal Mechanical Fatigue," *Journal of Electronic Materials* Vol. 28 (1999), p. 1288.

[9] Vianco, P. and Rejent, J., "A Methodology to Establish Baseline Metrics for Assessing the Isothermal Aging of Sn-Pb Solder Interconnects," *Soldering and Surface Mount Technology* Vo. 14 (2002), p. 26.

[10] Vianco, P., Hopkins, P., Erickson, K., Frear, D., and Davidson, R., "Modeling Non-Isothermal Intermetallic Layer Growth in the 63Sn-37Pb/Cu Systems," Design and Reliability of Solders and Solder Interconnections ed. by R. Mahidhara, et al., TMS (Warrendale, Pa; 1997), p. 161.